Synergistic Systems for Spacecraft Attitude Control

Renuganth Varatharajoo, Aznijar Ahmad Yazid, Mohd Ramly Ajir
Spacecraft System, Department of Aerospace Engineering, Universiti Putra Malaysia
43400 UPM Serdang Selangor.

ABSTRACT

The synergistic system design could be an attractive approach for future spacecraft to cope with their demands. The idea of combining the Attitude Control System and the conventional Electrical Power System is presented here. In this article, the Combined Energy and Attitude Control System (CEACS), a double counter rotating flywheel assembly in the pitch axis, is investigated for small satellites. The performance of CEACS is demonstrated for a selected configuration and mission. Another idea of incorporating the Attitude Control System into the Thermal Control System is also investigated. The Combined Attitude and Thermal Control System (CATCS) consisting of a "fluid wheel" and permanent magnets, couples an existing onboard temperature gradient with the magneto-hydrodynamic (MHD) effects for its operation. The performance of CATCS is demonstrated for a reference configuration and mission. The CEACS and CATCS are potential synergistic systems for the future spacecraft.*

Keywords : *Flywheel/fluid wheel/spacecraft attitude control*

INTRODUCTION

Synergisms for spacecraft describe the linking or merging of different subsystems in order to achieve a better overall performance, e.g. in reliability, mass saving or even for enabling a certain mission. In coming years, the projected power requirements for space missions will be increasing. With the current energy densities (5-20 Wh/kg), the conventional energy storage system (electrochemical battery) could most probably be insufficient to handle this task [1]. Therefore, having reasonably high energy densities (60 Wh/kg), the flywheels are proposed as the alternative energy storage device for the future spacecraft. These flywheels can also simultaneously serve as attitude actuators in the spacecraft, forming a "Combined Energy and Attitude Control System" (CEACS). Additionally, mass savings could also be achieved by such systems [2]. This concept has been proposed for bigger platforms in recent years, e.g. the International Space Station (ISS) [3]. In the present article, the idea is investigated for the small satellites. Generally, the CEACS should consist of a double counter rotating flywheel assembly, magnetic bearings, motor/generator units, and control electronics for the energy/attitude management.

Another possible synergistic effect for future spacecraft could be generated by the coupling of the thermal and attitude control systems, eventually having a "Combined Attitude and Thermal Control System" (CATCS). In a spacecraft that requires an active thermal control, an electric conducting fluid system could be used for the thermal and attitude control. Such a system would make use of the thermoelectric effects generated by the available onboard temperature gradient, and the magnetic fields from the permanent magnets for its operation. Thus, an excess onboard heat could be used by the CATCS for the spacecraft attitude and thermal management. Consequently, the power budget for these tasks could be suppressed.

This article is organized in the following manner: First, the miniaturisation design principle is viewed generally to verify the possibilities of down scaling the conventional flywheels for CEACS. Second, in section 3, the CEACS power/attitude architecture is presented along with the required transfer functions. Its performance is analysed through numerical treatments and is presented in section 4. In section 5, the CATCS is introduced together with its governing equations. The principal investigation in determining the capability of this system as an attitude actuator is by the determination of its response time. Thus, in section 6, the transient analysis is formulated. The performance analysis follows for the CATCS in section 7. In the final section, the conclusion for this study is drawn.

MINIATURISATION DESIGN PRINCIPLE

Generally, the conventional reaction or momentum wheels for

Table 1 : Satellite Dimension

Satellite Mass [kg]	Satellite Dimension [m]
2	$0.1 \times 0.1 \times 0.1$
10	$0.22 \times 0.22 \times 0.22$
50	$0.6 \times 0.6 \times 0.6$
100	$1 \times 1 \times 1$

-Flywheels' masses: 20 % of the satellite's mass.

-Flywheel size: X % of the satellite's dimension.

-$t_{eclipse}$ = 36 minutes.

-Satellite mass m ≈ Satellite power P (empirical).

$$-\Omega_{\max} = \sqrt{\frac{2 P t_{eclipse}}{I_W}}$$

*German Patent Rights **DE 10230349. A1,** German Patent Rights **DE 10230350. A1,** and German Patent Pending (2003)*

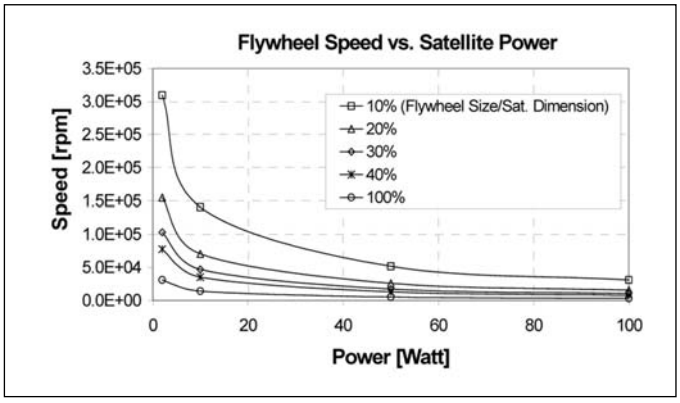

Figure 1: Requested speeds for each flywheel.

bigger satellites could be miniaturised for the small satellite applications. However, the CEACS's flywheel dimension is governed by the power requirement, mass and volume of a satellite. An overview on the relationship is envisaged based on the assumptions in Table 1.

The maximum requested flywheel speed Ω_{max} becomes the crucial parameter for CEACS. Figure 1 shows the quested relationship for different satellites. It can be seen that the flywheel speed increases drastically with the decrease in its size. This indicates that miniaturising the conventional flywheels for CEACS would result into very high rotational speeds. Therefore, the CEACS's flywheel dimension for small satellites should be increased to achieve higher inertia. Eventually, the operating flywheel speed could be suppressed between 40 000 rpm and 60 000 rpm. Moreover, this speed range is achievable with the currently available technology and is sufficient for the small satellite missions [4].

Composite rotors are mandatory for CEACS as they are very much stronger than metal rotors at high speeds. The design of such rotors can be implemented according to Kirk and Sung [5, 6]. Both investigators have focused mainly on the stress analysis for composite rotors. The dynamic analysis (rotor natural frequency) was not described in their investigations. For the small satellites (e.g. <120 kg), single layer composite rotors are found to be able to sustain the stresses (longitudinal and transverse), and to satisfy the energy requirements at about 50 000 rpm. The strength of these rotors can be further increased by using multi-layer configurations [5, 6]. As a result, the rotors can be operated at higher speeds so that their mass budgets could be further reduced. It has been found that even though the strength of the rotors can be increased, their dynamic behavior (eigenvalues) remains to be critical in the high-speed regimes [7]. The performed numerical treatments with a finite element software (ANSYS™) also revealed that the first natural frequency still appears around 50 000 rpm even with the multi-layer rotors. This is due to the thin structure/dimension of the rotors. This dimension could not be drastically altered as it is optimized corresponding to the mass allocation of the rotors. Therefore, the use of a single layer rotor is retained, and it is found to be sufficient for the small satellites.

CEACS CONTROL ARCHITECTURE

The CEACS control design can be implemented either based on the speed controlled mode or the torque controlled mode. The speed controlled mode is selected herein to minimise the steady state sensitivity of possible torque gain errors, especially coming from the differences in the flywheels' inertias and motor/generator constants.

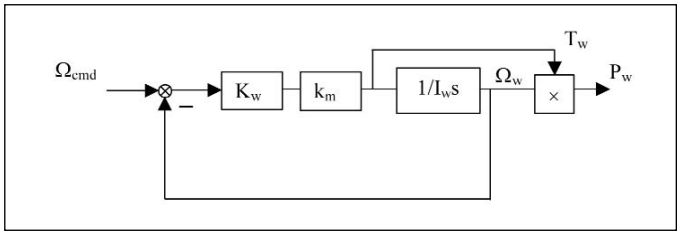

Figure 2: A single flywheel speed control loop

Figure 2 shows the speed control loop of a single flywheel system. From Figure 2, the transfer functions for the resulting speed Ω_w and the exerted torque T_w on a satellite are

$$\frac{\Omega_w}{\Omega_{cmd}} = \frac{K_w k_m}{K_w k_m + I_w s} = \frac{1}{1+\tau_w s} \tag{1}$$

and

$$\frac{T_w}{\Omega_{cmd}} = \frac{I_w s}{1+\tau_w s} \cdot \quad . \tag{2}$$

The transfer function for the output power P_w corresponding to the input speed command Ω_{cmd} is

$$\frac{P_w}{\Omega_{cmd}} = \frac{T_w \Omega_w}{\Omega_{cmd}} = \frac{I_w s \Omega_w}{(1+\tau_w s)} . \tag{3}$$

In Figure 2 the flywheel friction term is neglected as the magnetic bearing is used for supporting the rotor. Nevertheless, some other energy losses (e.g. iron losses: eddy-current, hysteresis, etc.) will be macroscopically included in the global charge/discharge efficiency of the system. Additionally, the vacuum compartment for CEACS omits the presence of air drag/friction on the flywheel.

In this investigation, the time constant chosen for the speed control loop is $\tau_w = 2\,s$, and for the motor/generator constant, which gives a proportional relation between the control current and resulting torque, $k_m = 1$ is assumed. As the torque T_w is exerted on the satellite body, an identical counter-rotating partner must be employed to compensate for the torque produced during the charging and discharging phases. The architecture for a double flywheel is presented in Figure 3.

From Figure 3, the transfer function for the total system power P_{system} with respect to the torque energy command $T_{energy.cmd}$ is

$$\frac{P_{system}}{T_{energy.cmd}} = \frac{K_1 I_{w1} \Omega_{w1}}{(1+\tau_{w1} s)} + \frac{K_2 I_{w2} \Omega_{w2}}{(1+\tau_{w2} s)} , \tag{4}$$

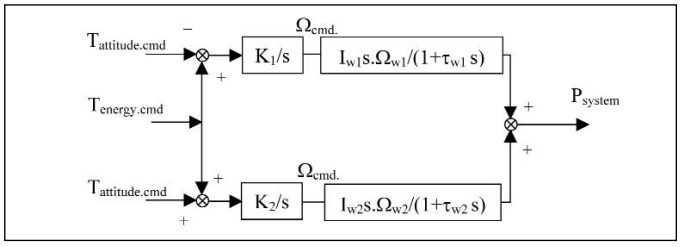

Figure 3 : A double flywheel power loop

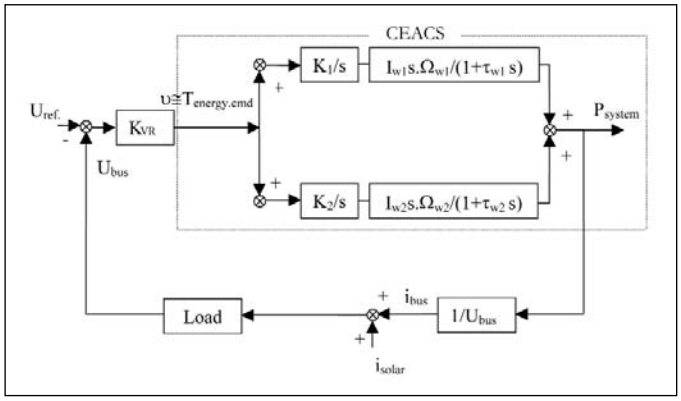

Figure 4: Power management by CEACS

where, for an ideal system, $I_{w1} = I_{w2} = I_w$, $\tau_{w1} = t_{w2} = t_w$, and $K_1 = K_2 = K$. Further, the integrators' gains in this analysis are set to one, thus $2KI_w = 1$.

The CEACS can be integrated on the satellite bus as shown in Figure 4. This design offers a tightly regulated bus voltage. Moreover, a bus voltage regulator KVR can be used to determine the charging and discharging phases without an additional switching equipment. As soon as the bus voltage U_{bus} gets higher than the bus reference voltage U_{ref}, a positive torque command by the regulator will result into a charging operation. In the case that U_{bus} drops below U_{ref}, a negative torque command will discharge the flywheels. In this investigation, the nominal bus reference voltage is assumed to $U_{ref} = 28\ V$.

On the other hand, the attitude control loop can be implemented as shown in Figure 5. By introducing a filter *F(s)* in Figure 5, the transfer functions developed are valid for the single (angle θ_{sat}) and double (including angle rate ω_{sat}) attitude feedbacks. As shown in Figure 3, the desired attitude control torque is achieved by slowing-down one flywheel and speeding-up its counter rotating member. The attitude controller selected for this application is a Proportional-Derivative (PD) type, which shows good agreements with the stability aspects. Setting the integrators' gains equal to one in Figure 3, and assuming that the flywheels are identical, the dynamics for this attitude actuator is

$$\frac{T_S}{\upsilon} = \frac{1}{1+\tau_w s}. \tag{5}$$

As a result, the transfer function for the satellite's dynamics in Figure 5 yields

$$\frac{\theta_{sat}}{\theta_{ref}} = \frac{1}{1+\frac{K_D}{K_P}s+\frac{I_{sat}}{K_P}s^2+\frac{I_{sat}\tau_w}{K_P}s^3}, \tag{6}$$

where $F(s)$ is $\dfrac{1}{1+(K_D/K_P)s}$.

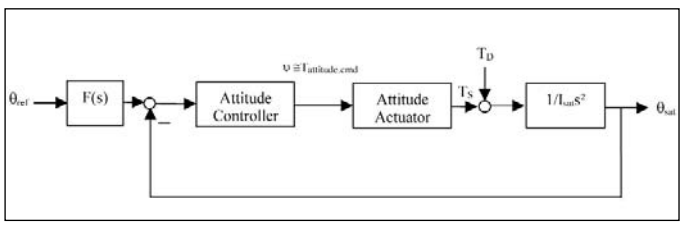

Figure 5: Attitude Control Architecture

CEACS PERFORMANCE

To facilitate the evaluation procedure, a reference mission is chosen as below:

- Mission duration: 5 years.
- Circular orbit at 500 km with an inclination of 53°.
- Period: 95 minutes with 36 minutes of eclipse.
- Satellite mass: 100 kg for 1 m^3 of volume.
- Attitude accuracy: Pitch (Y) < 0.2°.
- Maximum external disturbance torque $T_{D.pitch} = 6.15 \times 10^{-5}\ Nm.$
- Power requirement: 98 W.

The optimised rotor inertia I_w for this mission is about *0.0155 kgm²,* which corresponds to the inner and outer radii of *0.1137 m* and *0.1430 m*, respectively. On the other hand, the selected proportional and derivative attitude control gains are $K_P = 0.0252$ *Nm/rad* and $K_D = 0.9489$ *Nms/rad*, respectively. The closed loop poles are in the left side of the imaginary axis; hence, the system is stable. In addition to that, this particular mission is assumed to be a bias momentum stabilised type. Therefore, the CEACS is also requested to provide about *6 Nms* of bias momentum or a minimum bias speed of about *400 rad/s* along the pitch axis. The evaluation starts for an ideal CEACS considering only the external disturbance torques acting on the satellite. The initial speed for one of the flywheels was set to *1000 rad/s* in the numerical simulation using Matlab™. The charge/discharge efficiency for the flywheels was kept to about *80%* [4]. And, a depth of discharge (DoD) of about *90%* was maintained for the operational reasons. In Figures 6 (a) and (b), the flywheels' speeds increase during charging and decrease during discharging operations as expected. These results justify that the flywheel speed range posited in section 2 is hence suitable (below 50 000 rpm). Figure 6 (d) shows that the energy demanded (≈ *60 Wh*) during the eclipse phase is fulfilled by the system. Additionally, the attitude accuracy and the bias momentum remain within their budgets, see Figures 6 (e) and (c), respectively.

The second test case is for a non-ideal CEACS. The identified internal gain errors, which disturbance the system, are from the relative differences in motor/generator constants and flywheels' inertias. On the other hand, the relative misalignment (e.g. *0.1°*) has an impact on the transverse axes of the flywheels' rotational axis; however, this can be overcome with the recent technology advances in the magnetic bearings [4]. Therefore, the system was tested for a relative motor/generator constant difference of *0.5%* and a relative difference in flywheels' inertias of *0.2%* [2]. Figure 6 (f) shows the impact of these errors, which causes the attitude accuracy to exceed its pointing budget. However, the attitude improved after the control loop stiffness was tightened accordingly, see Figure 6 (g). The CEACS shows good performance for the reference mission.

THE CATCS

The basic idea to combine the thermal control system and the attitude control system is by utilizing an electrical conductive fluid, which circulates in a closed loop to serve as a "heat conductor" and a "momentum generator". Thus, the conventional heat pipes

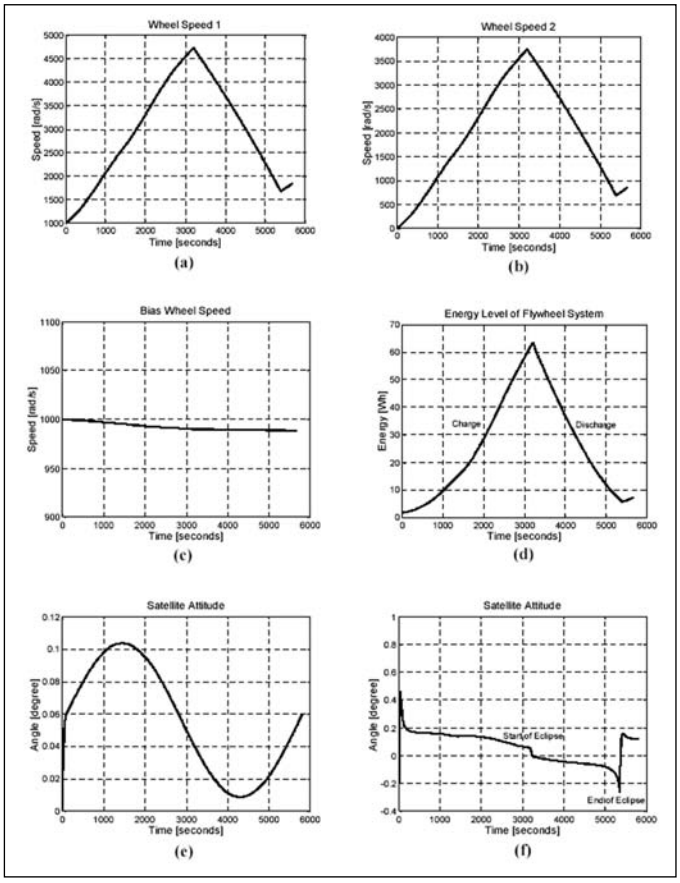

Figure 6: CEACS Performance

could be replaced by a duct system in which the fluid with a reasonable heat transfer coefficient circulates, and simultaneously generates reaction torques for the attitude control. The fluid motion could be influenced by a variation of the external and internal effects, e.g. electric and magnetic fields, and temperature gradients. The concept makes use of the existing temperature gradient in satellites to create a flow through the coupling of the thermoelectric and magnetic fields. The thermoelectric current can be generated by the temperature gradient between metal pairs. Hence, when a magnetic field is introduced near the generated electric current, a fluid flow is induced.

Two configurations are proposed for CATCS, see Figures 7 (a) and (b). The former benefits from the internal heat sources (payloads) and the latter benefits from an external heat source (Sun). These configurations allow an active heat dissipation to the neighboring satellite walls, which will eventually avoid thermal stresses on the satellites. Additionally, this method is independent from the natural convection phenomena, and enhances the heat transport activity. In both configurations, the fluid velocity is controlled by varying the distance between the permanent magnets and fluid housing. This task can be executed by engaging the linear motors to position the magnets [8]. The system details are given in Figure 7 (c). The working fluid selected is gallium, which has a melting point at *303 K*. In fact, this value can be easily dropped by adding the indium (*24%*) and tin (*16%*) compounds [9]. The thermoelectric generator selected as an example is cobalt with an absolute thermoelectric power ΔS of about *-35 μV/K*. Since the liquid-metal gallium is active towards cobalt, the stainless steel is chosen for the fluid housing. Both the materials, gallium and stainless steel, have no absolute thermoelectric powers, but they are reasonable electric and heat conductors. And, the permanent magnets chosen for the setup are Neodymium-Iron-Boron ($Nd_2Fe_{14}B$) type [10].

The crucial parameter to be estimated first is the maximum fluid velocity V_{max}. The working principle of this system is that the pressure drop due to the duct friction Δp_{loss} must be balanced by the total pressure of the MHD pumps $n\Delta p_{pump}$. Therefore, the Bernoulli's equation for this closed fluid system yields

$$\Delta p_{loss} = n\,\Delta p_{pump}\,. \tag{7}$$

The equivalent pressure provided by a MHD pump is induced by the Lorentz force ($F_L = b\ i\ B$) over a cross section ($A = h\ b$).

$$\Delta p_{pump} = \frac{F_L}{A}\,. \tag{8}$$

Another required parameter to be calculated is the generated thermoelectric current i_{local}, which can be estimated with the following equation,

$$i_{local} = \sigma_{ec}\,\frac{A_e}{b}\,\Delta S\,\Delta T\,, \tag{9}$$

where the cross section A_e is: the mean circumference of duct l_f times height h. It is assumed that a MHD compartment has a particular length $l_f \approx 0.05\ m$. Subsequently, the estimated current is about *80 A* corresponding to an assumed system temperature gradient ΔT of *50 K*. For the magnetic flux density *B = 0.5 T*, eq. (7) yields for the maximum fluid velocity V_{max} *= 1.07 m/s*. As a result, the corresponding angular momentum is about *0.95 Nms*. Since the CATCS will be used as "fluid reaction wheel", the quest for its response time will be the prime analysis as reflected in the next section.

TRANSIENT RESPONSE

The CATCS consists of the MHD and classical fluid flows (see Figure 6), which will be characterised respectively in the following. For the reference case, the Hartmann number *Ha >>1*. Thus, the Hartmann flow and MHD Couette flow solutions show the velocity and current variations are localised in a very thin layer (close to the wall), whose thickness is of the order of *h/Ha* [11]. Hence, the system's time response is dominated by the evolution of the core velocity V_θ in the core region. Taking into account the Hartmann properties and the current density in the core region for parallel flows, the Navier-Stokes equation can be solved for the core velocity. In seeking an analytical solution to the transient response, the convection, pressure, viscosity and gravity terms are neglected. The solution for the core velocity in Laplace form yields.

$$V_\theta(s) = \frac{I}{2 l_\theta \sqrt{\sigma_{ec}\,\rho\,\nu}} \left(\frac{1}{1 + (\frac{h^2}{\nu\,Ha})\,s} \right). \tag{10}$$

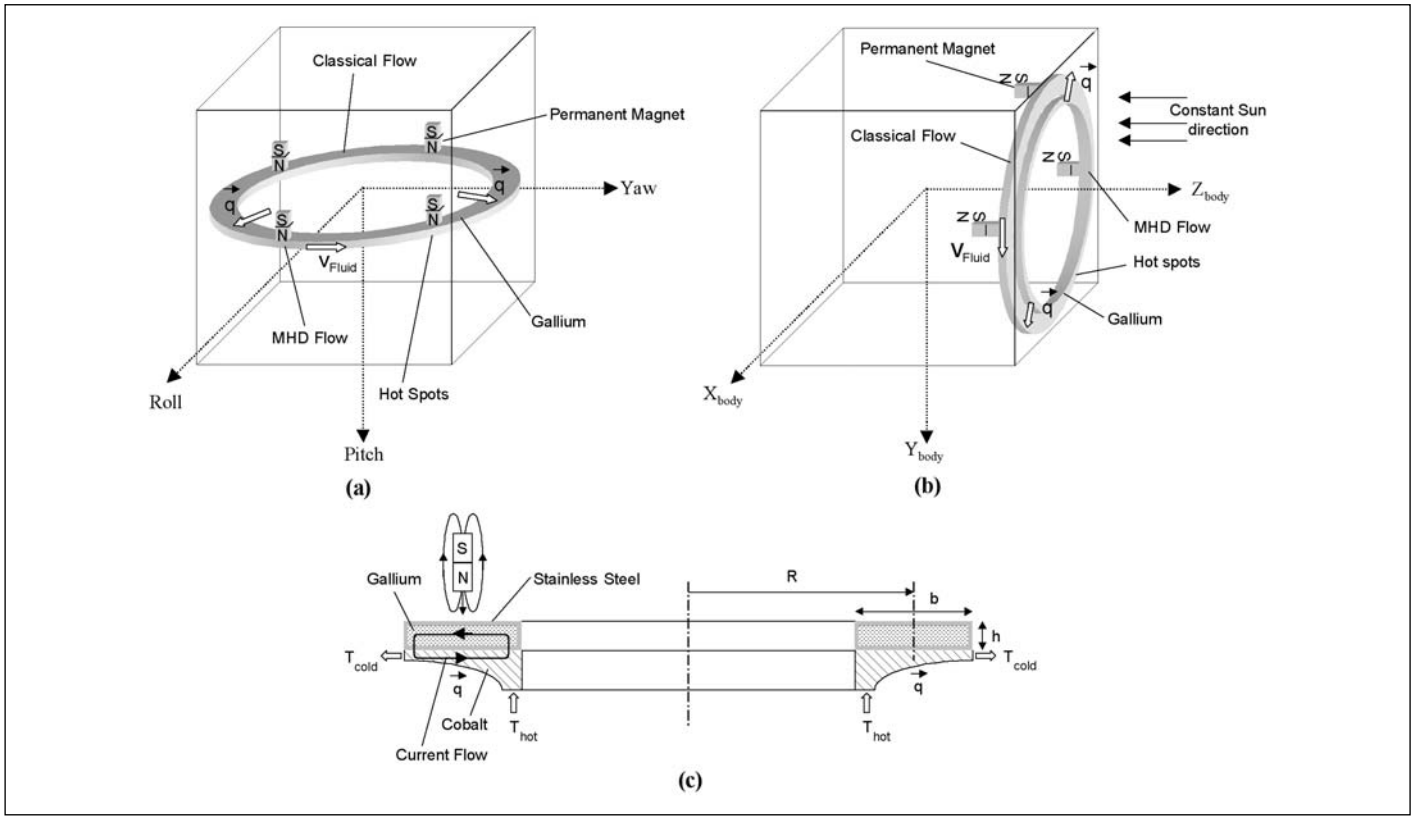

Figure 7 : CATCS Configuration. Setup details: Radius R = 0.5 m, height η = 5 mm, width b = 20 mm, mass μ = 1.86 kg, number of MHD pumps η = 4, fluid inertia If = 0.46 kgm², and heat flow q

The core velocity has an exponential function with a response time τ_{mhd} of $h^2/\nu Ha$. For the reference configuration, the estimated time constant is $\tau_{mhd} = 0.68\ s$. In order to determine the response time of the complete system, this transient analysis is continued for the classical fluid flow.

The final pressure of the MHD pumps p_{final} must balance the friction pressure drop in order to achieve the intended fluid velocity V_{final}. Therefore, the transient flow can be expressed in the following

$$\frac{\partial V}{\partial t}\rho l = p_{final}\left(1-\frac{V_{ins}^2}{V_{final}^2}\right), \qquad (11)$$

where V_{ins} is the mean instantaneous fluid velocity. Applying the boundary conditions, $V_{ins} = 0$ at $t = 0$, and noting that the exponential velocity profile attains 99% of the V_{final} in a finite time, this equation yields for the quested response time.

$$\tau_{cls} = 2.646\frac{\rho\, l V_{final}}{p_{final}}. \qquad (12)$$

The response time solves to $\tau_{cls} = 1.2\,s$. Thus, the total response time for CATCS is: $\tau_f = \tau_{mhd} + \tau_{cls} = 1.88\,s$. With this remarkable response time, the CATCS attitude control architecture can be envisaged.

CATCS PERFORMANCE

Before embarking on the performance evaluation, the CATCS attitude control architecture has to be implemented first. The attitude control design in Figure 5 is radically similar for CATCS. Only the dynamics of this actuator need to be established, see Figure 8.

From Figure 8, the displacement d, induced magnetic flux density B and resulting torque T_f are the physical constants describing the drivers. Their dependencies are given by the linear motor constant k_L, induced flux density constant k_B, and resulting torque constant k_T, respectively. The system gains are: $K_C = 1/n$, and the drivers' constants are held as below for an ideal system

$$k_{L1} = k_{L2} = k_{L3} = k_{L4} = k_L,$$
$$k_{B1} = k_{B2} = k_{B3} = k_{B4} = k_B,$$
and $$k_{T1} = k_{T2} = k_{T3} = k_{T4} = k_T.$$

The product of these constants is defined as: $k_L \times k_B \times k_T = k_G$. And, the ε in Figure 8 represents the system torque accuracy: $\varepsilon = 1 \pm \varepsilon_T$, where ε_T is the internal torque gain errors. For an ideal system, ε_T would be equal to zero so that $\varepsilon = 1$. The attitude controller selected is a Proportional-Integral (PI) type, which fulfils the stability aspects as well. Thus, the transfer function for the satellite's dynamics is

$$\frac{\theta_{sat}}{\theta_{ref}} = \frac{1}{\left(1+\frac{K_P}{K_i}s+\frac{I_{sat}}{K_i k_G \tau_f}s^2+\frac{I_{sat}}{K_i k_G}s^3\right)}, \qquad (13)$$

where $$F(s) = \frac{1}{1+(K_P/K_i)s}.$$

With these equations, the control architecture is amenable for the numerical treatment using Matlab™. The reference mission

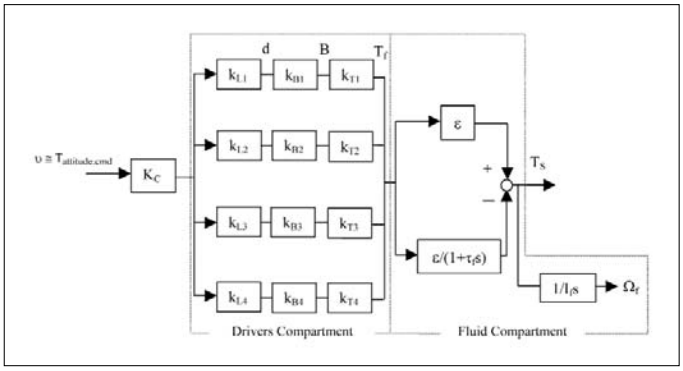

Figure 8: CATCS Actuator Compartment

defined in section 4 is retained for the CATCS performance analysis. The chosen attitude control gains are $K_P = 0.8$ *Nm/rad*, $K_i = 0.011$ *Nm/s*, and k_G is regarded as unity so that the desired and exerted torque commands are directly proportional. The system's response time τ_f was set to *2 s*. The linear motors' delays (e.g. *50 ms*) were also considered in the simulation. The ideal CATCS simulation results are depicted in Figures 9 (a) and (b). The satellite's attitude is within the pointing budget ($\theta_{sat} < 0.2°$), see Figure 9 (a). In Figure 9 (b), the fluid velocity attains the maximum velocity after about 5 operational orbit periods. To reset this velocity, the available standard desaturating methods can be engaged [12].

The second test case is for a non-ideal CATCS. Three torque gain errors are identified for this analysis, e.g. from the linear motors, permanent magnets, and the temperature instability in the MHD compartments. For the motors, about *4%* are assumed for the torque constants' differences. On the other hand, the temperature surrounding the magnets influences their magnetic flux densities *B* acting on the MHD compartments. For the $Nd_2Fe_{14}B$ magnets, this temperature dependency is about *0.15% / °C* [10]. Additionally, the vacuum environment is assumed to have a maximum gradient/margin of *10°C* [13]. Therefore, this would induce *1.5%* difference in the resulting control torque. Finally, the temperature variation in the MHD compartments is held about $\pm$ *2 K* with respect to the system's temperature gradient of *50 K* [14]. This

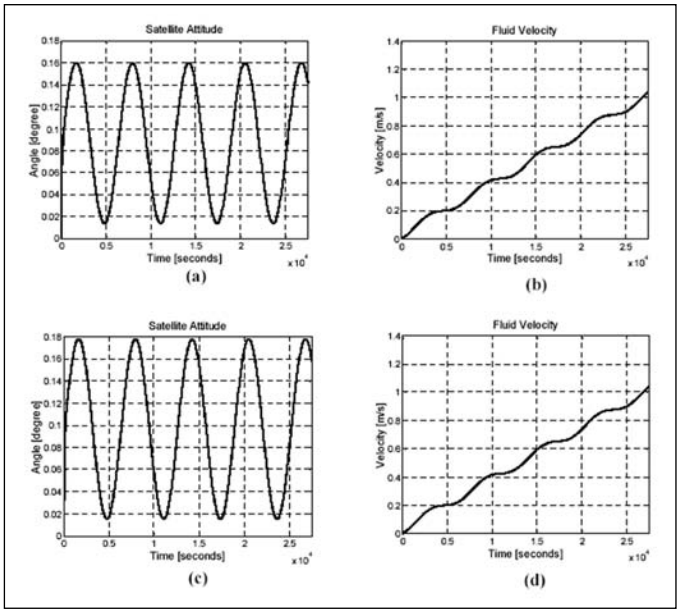

Figure 9: CATCS Performance

would account for about *4%* of difference in the generated thermoelectricity, and is proportional to the system's torque gain error. So, macroscopically, the total system torque gain errors ε_T would account for about *9%*. For this non-ideal test case, all the system gains were retained as in the ideal simulation. Despite the gain errors, the results pertaining to the non-ideal analysis show that the attitude accuracy and the fluid velocity are still within their nominal limits, see Figures 9 (c) and (d), respectively. Nevertheless, if desired, the attitude accuracy can be increased by tightening the stiffness of the attitude control loop.

So far only the attitude control performance for CATCS is discussed. It is also necessary to view its heat transport aspects. For example, having a temperature gradient of *5 K* (hot and cold satellite walls) together with the estimated mass flow (e.g. *0.3 kg/s*), the system can transport about *560 W* of heat from an exposed area of *0.01 m²*. Thus, the CATCS has a reasonable heat transport capability. On the other hand, the conventional heat pipes have good heat transport capabilities as well. However, in some cases their mass could reach up to *1 kg* or more depending on the types [15, 16]. As a result, the total mass budget for the conventional heat pipes and a reaction wheel (e.g. *0.4 Nms*) could reach up to *2.7 kg* [15, 16, 17]. This indeed has a significant impact on the overall spacecraft mass budget. Instead, the entire CATCS mass budget would account for about *2.5 kg*. Moreover, through the effects of synergism, additional mass savings could be obtained. For example, the CATCS requires only small amount of electrical power for the motors (e.g. *6.4 W* for 4 units) so that the performance of the solar panels and batteries could be reduced in terms of their masses.

It is evident that the CATCS is susceptible to the temperature variations, especially in the MHD compartments. To alleviate this problem and to arrest such situations, the use of electrical heaters (e.g. thermofoils) becomes desirable. These heaters are extremely lightweight, and consume about *1 W* corresponding to the temperature per-heated mass, e.g. *15°C/kg* can be achieved in half an hour for cobalt [18]. Moreover, these thermofoils could be used to partially dump the excess solar power during the begin-of-life (BOL), which could eventually increase the system's thermoelectric generation capability. This coupling can be classified as an additional advantage of the CATCS. Further, to achieve even higher thermoelectricity, the use of better thermoelectric generators (e.g. bismuth) instead of cobalt can be envisaged. In fact, this could be also an approach for the satellites with lower on-board temperature gradients to employ the CATCS. In this investigation, it has to be noted that the magnetic flux densities used are only half of the theoretical value for the reference configuration. Hence, with only two $Nd_2Fe_{14}B$ magnets (e.g. *1 T*), the similar performance presented in this article can be achieved. As a result, the power and mass budgets for CATCS can be reduced accordingly.

CONCLUSION AND OUTLOOKS

The CEACS attitude and power management for a small satellite has been demonstrated in this article. The ideal and non-ideal CEACS performances coincide with the reference mission requirements. The CEACS is a promising alternative compared to the separate conventional attitude and power systems, especially for increasing the life of the LEO satellites. The second system,

CATCS, has also its own potentials. This system is suitable for the satellites that require an active thermal control to handle the excess on-board heat. The performances shown by the ideal and non-ideal CATCS also comply with the mission requirements. Moreover, the usage of the unwanted on-board heat for its operation brings the additional benefits for the satellites. Both systems, CEACS and CATCS, demand a stringent design procurement. However, with the current available technologies such systems are judiciously feasible. In order to achieve their formal operational statuses, further research will be concentrated on designing the prototypes. This would also allow the systems' gains or parameters to be characterised profoundly. Finally, this investigation demonstrates the potential synergisms for the attitude control system, and offers a novel approach for designing the future spacecraft.

ACKNOWLEDGEMENT

The authors would like to thank R. Kahle and S. Fasoulas at TU. Dresden-Germany for their support. Financial aid from the Malaysian Government is also appreciated.

REFERENCES

[1] W. Robinson, et al., "Spacecraft Energy Storage System," *11th AIAA/USU Conference on Small Satellites*, Logan, Utah, 1997.

[2] P. Guyot, H. Barde, and G. Griseri, "Flywheel Power and Attitude Control System (FPACS)," *4th ESA Conference on Spacecraft Guidance, Navigation and Control System*, ESA-ESTEC, Noordwijk, 1999.

[3] C. M. Roithmayr, International Space Station Attitude Control and Energy Storage Experiment: Effects of Flywheel Torque, *NASA Technical Memorandum 209100*, 1999.

[4] H. Barde, "Energy Storage Wheel Feasibility Study," *4th Tribology Forum and Advances in Space Mechanisms*, ESA-ESTEC, Noordwijk, 2001.

[5] J. A. Kirk, J. R. Schmidt, G. E. Sullivan, and L. P. Hromada, "An Open Core Rotator Design Methodology Rotor," *Aerospace and Electronics Conference*, IEEE-NAECON, Dayton, 1997.

[6] K. H. Sung, K. Dong-Jin, and S. Tae-Hyun, "Optimum Design of Multi-ring Composite Flywheel Rotor Using a Modified Generalized Plane Strain Assumption," *Int. J. Mech. Sci.*, Vol. 43, pp. 993-1007, 2001.

[7] V. Renuganth and S. Fasoulas, The Combined Energy and Attitude Control System for Small Satellites – Earth Observation Missions, *Digest of 4th IAA Symposium on Small Satellites for Earth Observation*, ISBN 3896855697, Berlin, Germany, 2003.

[8] Linear Motor Data Sheet, Haydon, Waterbury, USA, 2002.

[9] S. Lee, "Liquid Metal Wetting of Metal Surfaces Using a DC Glow Discharge," *J. Korean Physical Society*, Vol. 29, pp. 257-260, 1996.

[10] Rare-Earth Permanent Magnets Data Sheet, Vacuumschmelze, Falkensee, Germany, 2001.

[11] R. Moreau, *Magnetohydrodynamics*, Kluwer Academic Publishers: Dordrecht, 1990, pp. 124 –126.

[12] J. R. Wertz, *Spacecraft Attitude Determination and Control*, Kluwer Academic Publishers: Dordrecht, 1994, pp. 202 and 648.

[13] J. W. Larson and J. R. Wertz, *Space Mission Analysis And Design*, Kluwer Academic Publishers: Dordrecht, 1997, pp. 416.

[14] Space Engineering - Mechanical – Part 1: Thermal Control, ECSS-E-30 Part 1A, ESA-ESTEC, 2000.

[15] Heat Pipes Data Sheet, Alcatel, Toulouse, France, 2000.

[16] Thermal Products and Solution Data Sheet, Dynatherm Corporation, California, USA, 1998.

[17] Momentum and Reaction Wheels Data Sheet, Teldix, Heidelberg, Germany, 2000/2001.

[18] Thermofoils Heaters and Controller Data Sheet, Minco Products, Minneapolis, USA, 2002.

NOMENCLATURE

A	cross section
b	width
B	magnetic flux density
D	hydraulic diameter
ϕ	friction coefficient = $0.32\ Re^{-0.25}$
F_L	Lorentz force
h	height
Ha	Hartmann number = $\sqrt{\frac{\sigma_{ec}}{\rho\nu}}\,B\,h$
i_{bus}, i_{solar}, i_{local}	currents
I_w, I_f, I_{sat}	inertias
k_m	motor torque constant
K_i	attitude integral constant
K_d	attitude derivative constant
K_p	attitude proportional constant
K_w	flywheel proportional constant
l_θ, l_f	longitudinal length
ν	number of pumps
P	power
Re	Reynolds number = $\frac{VD}{\nu}$
t	time
T	torque command
T_D	external disturbance torques
T_S	torque exerted on the satellite body
U	voltage
V	velocity
Δp_{loss}	friction pressure = $f\,\frac{2\pi R}{D}\,\frac{\rho}{2}\,V^2$
ΔS	thermoelectric power
ΔT	temperature gradient
θ_{ref}, θ_{sat}	reference and true satellite attitudes
$\upsilon = T_{attitude.cmd}$	proportional torque command
ν	kinematic viscosity ($\nu = 3.49 \times 10^{-7}\ m^2\ s^{-1}$)
ρ	density ($\rho = 5907\ kgm^{-3}$)
σ_{ec}	electrical conductivity ($\sigma_{ec} = 3.7 \times 10^6\ Ohm^{-1}m^{-1}$)
Ω	flywheel speed